







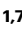




# $\beta$ -amyloid monomer scavenging by an anticalin protein prevents neuronal hyperactivity in mouse models of Alzheimer's Disease

Received: 25 January 2023

Accepted: 2 July 2024

Published online: 10 July 2024

 Check for updates

Benedikt Zott <sup>1,2,3,4</sup> , Lea Nästle<sup>5</sup>, Christine Grienberger <sup>1,6</sup>, Felix Unger <sup>1,2,3</sup>, Manuel M. Knauer <sup>1</sup>, Christian Wolf <sup>1,2</sup>, Aylin Keskin-Dargin<sup>1</sup>, Anna Feuerbach<sup>5</sup>, Marc Aurel Busche <sup>1,7</sup>, Arne Skerra <sup>5</sup>  & Arthur Konnerth <sup>1,4</sup> 


Hyperactivity mediated by synaptotoxic  $\beta$ -amyloid (A $\beta$ ) oligomers is one of the earliest forms of neuronal dysfunction in Alzheimer's disease. In the search for a preventive treatment strategy, we tested the effect of scavenging A $\beta$  peptides before A $\beta$  plaque formation. Using in vivo two-photon calcium imaging and SF-iGluSnFR-based glutamate imaging in hippocampal slices, we demonstrate that an A $\beta$  binding anticalin protein (A $\beta$ -anticalin) can suppress early neuronal hyperactivity and synaptic glutamate accumulation in the APP23xPS45 mouse model of  $\beta$ -amyloidosis. Our results suggest that the sole targeting of A $\beta$  monomers is sufficient for the hyperactivity-suppressing effect of the A $\beta$ -anticalin at early disease stages. Biochemical and neurophysiological analyses indicate that the A $\beta$ -anticalin-dependent depletion of naturally secreted A $\beta$  monomers interrupts their aggregation to neurotoxic oligomers and, thereby, reverses early neuronal and synaptic dysfunctions. Thus, our results suggest that A $\beta$  monomer scavenging plays a key role in the repair of neuronal function at early stages of AD.

How to halt Alzheimer's disease (AD) and the associated cognitive decline and memory loss remains one of the major challenges in the research of brain diseases. According to the  $\beta$ -amyloid (A $\beta$ ) hypothesis, A $\beta$  peptides and, especially, their soluble aggregates comprising dimers and small oligomers are the most toxic agents that perturb the integrity of neuronal structure and function<sup>1</sup>. A $\beta$  peptides were also shown to cause inflammation<sup>2</sup>, tau hyperphosphorylation<sup>3</sup>, and, ultimately, cell death<sup>4</sup>. Given these observations, the depletion of A $\beta$  is expected to slow down or,

hopefully, even prevent the cognitive decline associated with AD in affected individuals.

Until relatively recently, treatment strategies aiming at the scavenging of A $\beta$  by passive immunization with antibodies have largely failed to show a significant deceleration of cognitive decline in clinical studies, in fact raising concerns about the amyloid hypothesis<sup>5</sup>. Similar discouraging observations were made in Alzheimer's mouse models<sup>6,7</sup>. There are several possible explanations for the general failure of these approaches, most prominently an inadequate timing of the

<sup>1</sup>Institute of Neuroscience, Technical University of Munich, Munich, Germany. <sup>2</sup>Department of Neuroradiology, MRI hospital of the Technical University of Munich, Munich, Germany. <sup>3</sup>TUM Institute for Advanced Study, Garching, Germany. <sup>4</sup>Munich Cluster for Systems Neurology (SyNergy), Munich, Germany. <sup>5</sup>Chair of Biological Chemistry, Technical University of Munich, Freising, Germany. <sup>6</sup>Department of Biology and Volen National Center of Complex Systems, Brandeis University, Waltham, MA, USA. <sup>7</sup>UK Dementia Research Institute at UCL, University College London, London, United Kingdom.

 e-mail: [benedikt.zott@tum.de](mailto:benedikt.zott@tum.de); [skerra@tum.de](mailto:skerra@tum.de); [arthur.konnerth@tum.de](mailto:arthur.konnerth@tum.de)

therapeutic intervention after the brain has already undergone irreparable damage<sup>8</sup>. However, groundbreaking results were reported for the monoclonal antibodies (mAb), foremost Lecanemab, which preferentially binds protofibrils (>75 kDa soluble A $\beta$  aggregates) and significantly reduced cognitive decline in patients with early AD in a phase 3 study<sup>9</sup>.

Moreover, anti-A $\beta$  treatment at very early stages of development had positive outcomes in mouse models of  $\beta$ -amyloidosis. Thus, before A $\beta$  plaque formation, the prevention of extracellular A $\beta$  accumulation involving the use of  $\gamma$ -secretase inhibitors can effectively abolish neuronal hyperactivity<sup>10</sup>. This is relevant because a variety of studies in mice and humans have established that neuronal hyperactivity is probably the earliest form of neuronal dysfunction in the diseased brain<sup>10–17</sup>. This neuronal hyperactivity can be induced directly by the application of soluble A $\beta$  dimers, the smallest of all oligomers, and develops before A $\beta$  plaque formation<sup>10</sup>. Mechanistically, A $\beta$ -dependent neuronal hyperactivity has been linked to aberrant synaptic glutamatergic transmission<sup>18</sup> and impairments of inhibitory neurons<sup>19</sup>.

To untangle the conflicting results on the effectivity of A $\beta$  removal obtained from previous mouse studies<sup>6,10,20</sup>, we applied here an alternative approach based on the direct intracerebral application of A $\beta$ -binding anticalins<sup>21</sup>. We asked (1) whether A $\beta$  removal can restore neuronal and synaptic functions in mouse models of AD and (2) which species of A $\beta$  should be targeted for such an approach to be successful. Anticalins are proteins selected via phage display from a random library based on the human lipocalin protein scaffold and further engineered for optimal pharmacological properties. Anticalins exhibit very high target affinities and, in contrast to antibodies, a low immunogenic potential<sup>22</sup>. These properties make them potent A $\beta$  scavengers and the ideal tool to study the acute effects of A $\beta$  removal in vivo. Several A $\beta$ -binding anticalins with high affinities and specificities for the monomeric A $\beta$  peptide target have recently been described<sup>23</sup>, and their mode of tight complex formation with the central A $\beta$  epitope (Lys<sup>P16</sup> to Lys<sup>P28</sup>)—which is common to both A $\beta$ <sub>40</sub> and A $\beta$ <sub>42</sub> peptide species—was elucidated by X-ray crystallography<sup>24</sup>.

## Results

### A $\beta$ -anticalins prevent neuronal and synaptic dysfunctions

We produced the anticalin HIGA (dubbed A $\beta$ -anticalin) (Fig. 1A) in *Escherichia coli* and purified it to homogeneity as previously described (Fig. S1, materials and methods). The recombinant protein was biochemically characterized by ESI mass spectrometry and confirmation of binding activity towards the monomeric A $\beta$ (1–40) peptide using real-time surface plasmon resonance (SPR) spectroscopy. In our experimental setup, this A $\beta$ -anticalin solution was directly applied in vivo to the exposed hippocampal CA1 region<sup>10,18</sup> of 2–3-month-old *APP23xPS45* mice, at a stage preceding the formation of A $\beta$  plaques<sup>14</sup>. In this way, problems of brain delivery involving systemic application of this protein were circumvented. Simultaneously, we monitored changes in neuronal activity at single-cell resolution by using two-photon calcium imaging (Fig. 1B, C).

In line with previous observations made for the same animal model under similar conditions<sup>10</sup>, we registered a marked hyperactivity in a fraction of neurons under baseline conditions (Fig. 1D left). Local application of A $\beta$ -anticalin to the monitored CA1 neurons rapidly suppressed the hyperactivity (Fig. 1D middle, S2A). Notably, the A $\beta$ -anticalin effect on neuronal activity was largely reversible after a washout period of only 5–10 min (Fig. 1D right, S2B).

We have previously established that, at these early stages, neuronal dysfunction of hippocampal CA1 pyramidal neurons in mouse models of  $\beta$ -amyloidosis is characterized mainly by the emergence of hyperactive neurons, i.e., neurons with baseline activity levels of > 20 Ca<sup>2+</sup> transients/min<sup>10,18</sup>. A $\beta$ -anticalin treatment reduced the number of hyperactive cells in *APP23xPS45* mice to the same levels observed in wild-type mice (Fig. 1E). Moreover, a cell-by-cell analysis revealed that

A $\beta$ -anticalin treatment reduced neuronal activity levels in all neurons (Fig. 1F, Fig. S2 C–E), but most strongly affected the group of hyperactive cells (Fig. S3). Overall, in *APP23xPS45* mice treated with the A $\beta$ -anticalin, the neuronal activity distribution was indiscernible from that of wild-type mice (Fig. 1F).

Next, we estimated the minimum pipette concentration of the A $\beta$ -anticalin necessary to reduce neuronal activity levels. To this end, we applied decreasing concentrations of the A $\beta$ -anticalin to the CA1 hippocampal area of non-plaque-bearing *APP23* mice, a model of early AD, which, due to the lack of the PS mutation, develops plaques at a later age<sup>25</sup>. These mice, as the *APP23xPS45* mice, had high levels of hyperactive neurons (Fig. S4A) at the age of 4–8 months. The application of the A $\beta$ -anticalin markedly reduced neuronal activity levels in *APP23* mice, also at low pipette concentrations (IC<sub>50</sub> 75 nM) (Fig. S4B). However, as any solution applied from the point source of a pipette tip mixes rapidly with the interstitial fluid and becomes progressively diluted with increasing distance to the tip<sup>26</sup>, we expect the actual tissue concentration at the neuronal membranes to be much lower than in the pipette.

Control experiments demonstrated that the application of the A $\beta$ -anticalin did not alter activity levels in 2–4 month-old wild-type mice (Fig. S5, A and B), including those of the few neurons classified as hyperactive under baseline conditions (Fig. S5C). Likewise, the application of the recombinant human lipocalin 2, the protein from which the anticalin originates and which does not bind A $\beta$  in vitro<sup>23</sup>, in young *APP23xPS45* mice did not change the average number of Ca<sup>2+</sup> transients (Fig. S5D) or the number of hyperactive neurons (Fig. S5E).

Assuming that the A $\beta$ -anticalin effect is mediated by the reduction of toxic A $\beta$ -species in the brain, other means of A $\beta$  removal should also be effective in preventing neuronal hyperactivity in AD mice. Thus, we next investigated the action of the monoclonal Solanezumab antibody, which binds A $\beta$  at the same epitope as the A $\beta$ -anticalin<sup>24,27</sup>, has a high affinity for A $\beta$  monomers, but not oligomers or fibrils<sup>28</sup> and interacts with plaques in AD mouse models<sup>29</sup>. The application of Solanezumab into the hippocampal CA1 region of 4–8 month-old *APP23* mice decreased overall neuronal activity levels (Fig. S6, A–C), albeit less effectively than the A $\beta$  anticalin at the same concentration (Fig. S6D). In contrast, the application of a control IgG (Fig. S6E) or of the lipocalin 2 protein (Fig. S6F) was ineffective. Second, we applied the  $\gamma$ -secretase inhibitor LY-411575, which blocks the biosynthesis of the A $\beta$  peptide<sup>10,30</sup>. Indeed,  $\gamma$ -secretase inhibition markedly reduced the number of hyperactive cells and overall activity levels in 2–4 month-old *APP23xPS45* mice (Fig. S7 A, C, D), but not in wild-type mice (Fig. S7 B–E).

At the synaptic level, A $\beta$ -dependent neuronal hyperactivity is associated with the accumulation of extracellular glutamate<sup>18,31–33</sup>. To investigate whether the A $\beta$ -anticalin prevents this synaptic impairment, we performed two-photon imaging of synaptically released glutamate in hippocampal slices. First, using a viral vector, we expressed the fluorescent glutamate sensor SF-iGluSnFR<sup>34</sup> unilaterally in the hippocampal CA1 region of wild-type and *APP23xPS45* mice in vivo (Fig. 2A, top). After 2–3 weeks of viral expression, when the animals were 2–4 months old, we performed two-photon population imaging of synaptically evoked glutamate transients in the stratum radiatum of CA1 (Fig. 2A, bottom) by electric stimulation of the Schaffer collaterals<sup>35</sup>. We have previously reported that A $\beta$ -induced neuronal and synaptic dysfunctions are dependent on the level of baseline synaptic transmission<sup>18</sup>. Accordingly, we observed increasingly larger glutamate responses in the *APP23xPS45* mice compared to the wild-type animals for higher numbers of stimuli, but no significant difference for low numbers of pulses (Fig. 2B, C). The application of the A $\beta$ -anticalin in *APP23xPS45* mice reliably reduced the synaptically evoked glutamate transients to levels similar to those observed in wild-type animals (Fig. 2D, E). In control experiments, the application of the lipocalin 2 protein to *APP23xPS45* mice (Fig. 2F, Fig. S8A and C) or of

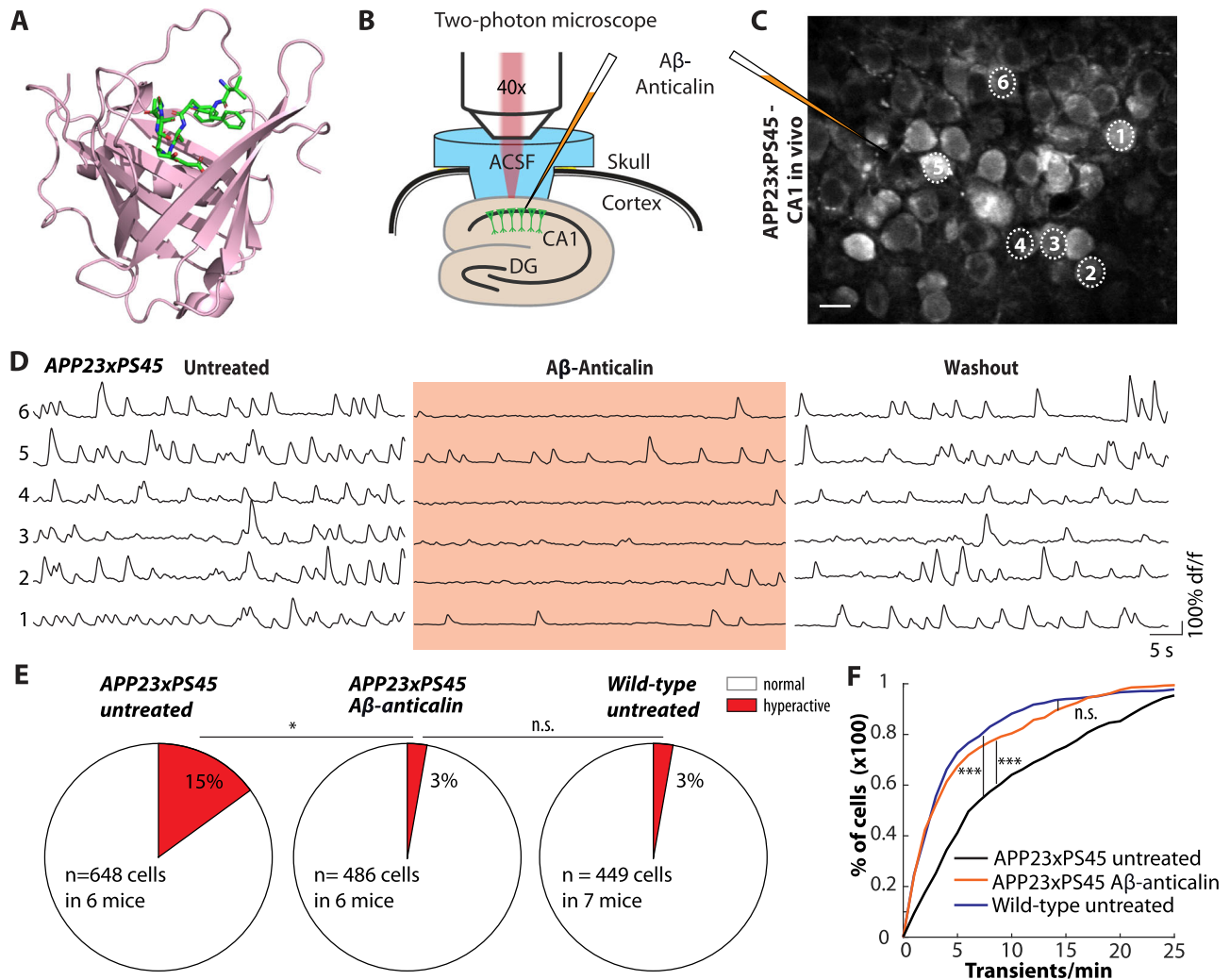


**Fig. 1 | Aβ-anticalin treatment suppresses neuronal hyperactivity in vivo.**

**A** X-ray structure (PDB ID: 4MVL) of the Aβ-anticalin with its β-barrel formed by eight anti-parallel β-strands and four hypervariable loops shown in ribbon presentation. The bound central segment of the Aβ(1-40) peptide is shown as sticks and colored green. **B** Two-photon imaging setup for in vivo imaging of the hippocampal CA1 region. The filled pipette for the application of the Aβ-anticalin is indicated in orange. ACSF, arterial cerebrospinal fluid; CA1, cornu ammonis I; DG, dentate gyrus. **C** Representative two-photon image of the pyramidal layer of the hippocampal CA1 region in a 2-month-old APP23xPS45 mouse after staining with the organic Ca<sup>2+</sup>-indicator Cal-520 AM. The injection pipette for the application of Aβ-anticalin is visible as a dark shadow on the left side of the image and

schematically outlined for clarity. Scale bar: 10 μm. **D** Ca<sup>2+</sup>-traces recorded from the six representative neurons labeled in **C** under baseline conditions (left), during the application of 10 μM Aβ-anticalin (middle) and after a washout period of 5 min (right). **E** Percentage of hyperactive cells (more than 20 Ca<sup>2+</sup>-transients per min) in untreated (left) and Aβ-anticalin-treated APP23xPS45 (middle) as well as in untreated wild-type animals (right). **F** Cumulative probability of the neuronal activity in untreated (black) and Aβ-anticalin-treated APP23xPS45 mice (orange) and in untreated wild-type mice (blue). \**p* < 0.05, \*\*\**p* < 0.001, n.s. not significant. Two-sided Wilcoxon signed-rank or rank sum test (E), two-sided Kolmogorov–Smirnov-test (F).

the Aβ-anticalin to wild-type mice (Fig. S8, B and D) did not change synaptically evoked glutamate transients. Collectively, these results establish that Aβ scavenging can reverse neuronal hyperactivity and synaptic glutamate accumulation.

### The Aβ-anticalin effect is not dependent on direct interaction with Aβ monomers or dimers

As an independent test for the anti-Aβ action of the Aβ-anticalin, we explored its effects on neuronal hyperactivity, which was experimentally induced through the direct application of Aβ to the hippocampus of 2–4 month-old wild-type mice<sup>10,18</sup>. For this experiment, we used the synthetic disulfide cross-linked Aβ dimer [AβS26C]<sub>2</sub>, which was shown to be a potent neurotoxic Aβ-agent in various assays, including neurite outgrowth<sup>3</sup>, the induction of long-term potentiation (LTP)<sup>36,37</sup> and neuronal hyperactivation<sup>10,18</sup>. It is important to note that in all these

assays, applications of [AβS26C]<sub>2</sub> faithfully reproduced the actions of human Aβ extracts, particularly those of natural Aβ dimers.

In line with earlier reports<sup>10,18</sup>, we first observed that the local application of [AβS26C]<sub>2</sub> to hippocampal CA1 neurons caused robust neuronal hyperactivation (Fig. 3, A and B). However, in contrast to the hyperactivity-blocking effect in the transgenic mice, the Aβ-anticalin did not have any blocking action on the [AβS26C]<sub>2</sub>-induced hyperactivity in wild-type mice (Fig. 3, C and D), and the actions of both applications were indiscernible (Fig. 3, E–G). While this result had to be expected based on the binding specificity of the Aβ-anticalin<sup>24</sup>, it is still remarkable as [AβS26C]<sub>2</sub> mimics the action of human Aβ dimers<sup>18</sup>. Thus, the experiment does not fully answer whether binding to monomers or dimers is necessary for the hyperactivity-reducing action of the Aβ-anticalin but may prompt further investigation of the interaction of the anticalin with different forms of Aβ.

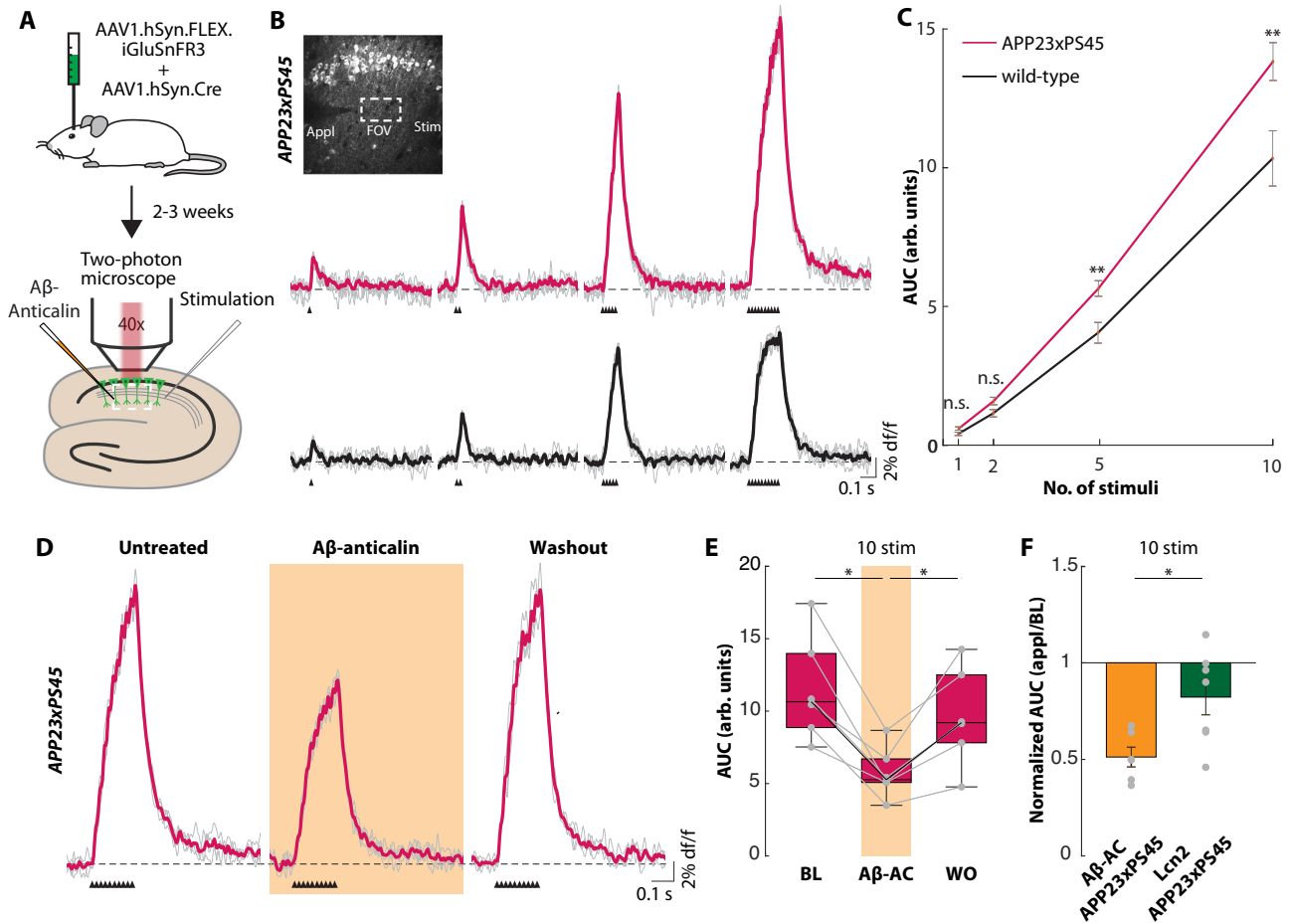


**Fig. 2 | The A $\beta$ -anticalin normalizes glutamate transmission in young APP23xPS45 mice.** **A** Schematic depiction of the SF-iGluSnFR-based glutamate imaging experiment. AAV injection in vivo (top) followed by in vitro population imaging (bottom). **B** Individual synaptically evoked glutamate transients (gray) and average (colored) from 2-month-old APP23xPS45 (top) or age-matched wild-type (bottom) mice for one, two, five and ten stimuli as indicated by black triangles. Inset: Two-photon image of iGluSnFR3-expressing CA1 pyramidal neurons and the positions of the pipettes. Appl: application pipette, Stim: stimulation pipette, FOV: field of view (scale bar: 50  $\mu$ m). **C** Area under the curve (AUC) of individual glutamate transients from wild-type (40 transients in  $N = 8$  slices) and APP23xPS45 (65 transients in  $N = 13$  slices) mice for one, two, five and ten stimuli. The error bars depict SEM. **D** Same as (B) for ten stimuli in a slice from an APP23xPS45 mouse

during baseline conditions (left), during the application of A $\beta$ -anticalin (10  $\mu$ M; middle) and after washout (right). **E** Summary data of the experiments in (D) for  $N = 6$  slices. Dots represent the mean area under the curve (AUC) of one slice. Box plot is represented as median and quartiles (bounding box). Whisker length is the distance to the furthest observation, but no further than 1.5 times the range from the median to the respective quartile. **F** Comparison of the AUC of glutamate transients during application of A $\beta$ -anticalin (10  $\mu$ M) or lipocalin 2 (10  $\mu$ M,  $N = 7$  slices) in APP23xPS45 mice normalized to the respective AUC under baseline conditions (mean  $\pm$  SEM). Source data for Fig. 2E, F are provided as a Source Data file. n.s. not significant, \* $p < 0.05$ , \*\* $p < 0.005$ . Two-sided Wilcoxon rank sum test (C, F), two-sided Wilcoxon signed-rank test (E).

It is well established that the A $\beta$ -anticalin binds A $\beta$  monomers with high affinity<sup>23,24</sup>. To determine the precise A $\beta$ -binding behavior of the A $\beta$ -anticalin, we performed size exclusion chromatography (SEC) of the A $\beta$ -anticalin alone and after mixture with freshly prepared A $\beta$  monomers. Compared to the isolated A $\beta$ -anticalin (Fig. 4, A and B), we observed a shift of the elution volume after combination with freshly prepared A $\beta$  monomers, corresponding to an increase in size by approximately 4.4 kDa (Fig. 4 C), in line with the known mass of 4430 Da for the A $\beta$  monomer.

In light of the strong affinity for monomers, we asked whether binding A $\beta$  monomers by the A $\beta$ -anticalin directly prevented their neurotoxic actions. In agreement with previous reports that A $\beta$  monomers do not impair LTP<sup>38</sup> or neurite outgrowth<sup>39</sup>, as well as the observation that human brain-derived monomers do not cause neuronal hyperactivation<sup>18</sup>, we observed that the administration of a freshly prepared synthetic A $\beta$  monomer solution in vivo did not cause neuronal hyperactivation in CA1 in 2–4 month-old wild-type mice (Fig. 4, D and E). To exclude a dose-dependent effect, we also performed two-photon imaging in acutely prepared hippocampal slices,

in which neuronal in vivo-like baseline activity had been induced by the application of bicuculline (Fig. S9). Under these conditions, the application of 1  $\mu$ M or 100  $\mu$ M solutions of the A $\beta$  monomers did not produce neuronal hyperactivation (Fig. 4, F and G).

### The A $\beta$ -anticalin prevents A $\beta$ oligomerization

As A $\beta$  monomers, themselves, did not induce neuronal dysfunction, we hypothesized that scavenging of the (nascent) A $\beta$  monomers by the A $\beta$ -anticalin must reduce the concentration of toxic A $\beta$  oligomers in the brain, either by preventing their formation or by facilitating their disintegration.

To surveil the aggregation behavior of A $\beta$ , we used a Thioflavin T (ThT) fluorescence assay as a probe for the formation of  $\beta$ -sheets<sup>40</sup> that are characteristic for A $\beta$  fibrils. We performed an A $\beta$  'aging' experiment, in which incubated A $\beta$  monomers immediately started forming  $\beta$ -sheet aggregates as demonstrated by a steep initial increase in the ThT-fluorescence, which decayed after approximately two hours, indicating completion of aggregate/fibril formation (Fig. 5A)<sup>41</sup>. The addition of the A $\beta$ -anticalin at the beginning of the incubation period,

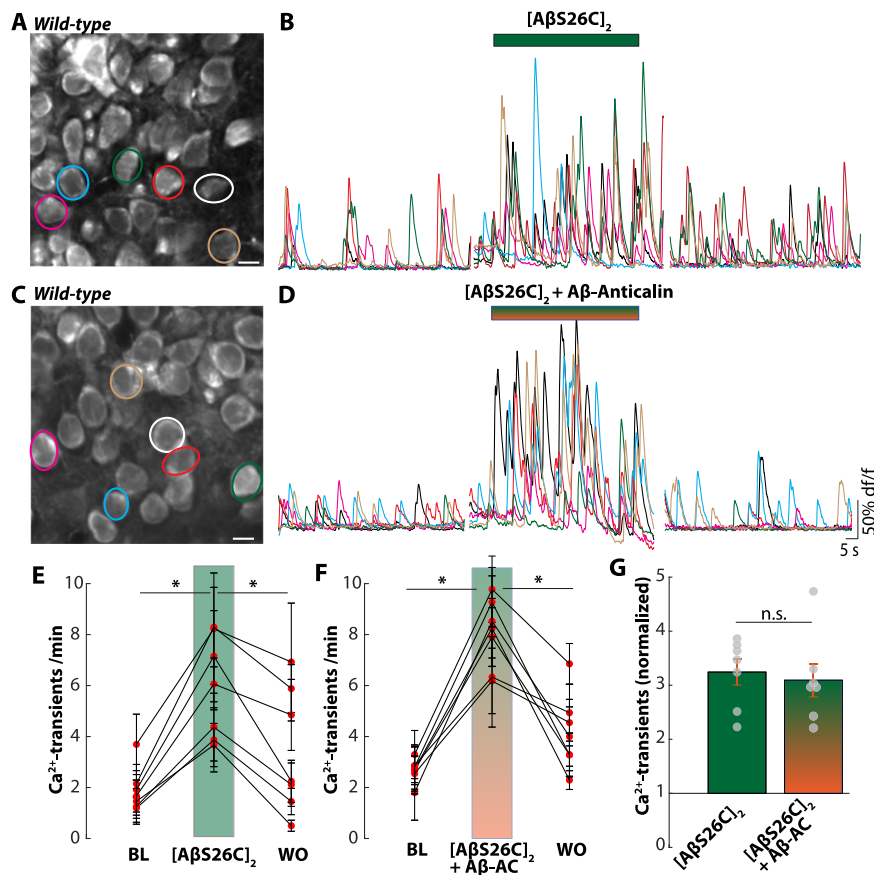


**Fig. 3 | Ineffectiveness of the A $\beta$ -anticalin to prevent A $\beta$ -dimer-induced neuronal hyperactivity.** **A** Representative two-photon image of the pyramidal layer of the hippocampal CA1 region in a 2-month-old wild-type mouse after staining with the organic Ca<sup>2+</sup>-indicator Cal-520 AM. **B** Superimposed representative Ca<sup>2+</sup>-traces of the six neurons cycled in **(A)** under baseline conditions (left), during the application of 500 nM [A $\beta$ S26C]<sub>2</sub> and after 5 min washout. The colors of the Ca<sup>2+</sup>-traces correspond to the circles in **(A)**. **C**, **D** same as **(A)** and **(B)** for the co-application of [A $\beta$ S26C]<sub>2</sub> (500 nM) and A $\beta$ -anticalin (1  $\mu$ M). **E** Summary data of the application experiments in **(B)** from  $N = 7$  mice. Each dot represents the mean number of Ca<sup>2+</sup>

transients per minute for all observed neurons in one mouse under baseline conditions (BL, left), during the application of [A $\beta$ S26C]<sub>2</sub> (middle), and after washout (WO, right). Data are presented as mean values  $\pm$  SEM. **(F)** Same as **(E)** for the experiment in **(D)**. **G** Number of Ca<sup>2+</sup>-transients during the application of [A $\beta$ S26C]<sub>2</sub> alone ( $N = 7$  mice) or mixed with A $\beta$ -anticalin ( $N = 7$ ), normalized to the respective mean baseline activity (mean  $\pm$  SEM). Source data for Fig. 3G are provided as a Source Data file. Scale bars: 5  $\mu$ m. n.s. not significant. \* $p < 0.05$ . Two-sided Wilcoxon signed-rank test (**E**, **F**), two-sided Wilcoxon rank sum test (**G**).

however, fully prevented the formation of ThT-positive A $\beta$  fibrils (Fig. 5B), as previously demonstrated by transmission electron microscopy<sup>23</sup>. In contrast, the addition of the A $\beta$ -anticalin after 90 min, i.e. after ThT-positive fibrils had formed, did not reduce fluorescence, indicating that preformed fibrils were not dissolved by the addition of the A $\beta$ -anticalin (Fig. 5C).

Based on the kinetics of A $\beta$  aggregate/fibril formation, we conclude that the freshly prepared synthetic A $\beta$  monomers immediately start forming aggregates and assume that A $\beta$  oligomers should arise as an intermediate step on the way to final fibril formation<sup>42</sup>. To test this, we applied the ‘aged’ A $\beta$  solution, i.e. A $\beta$ , which had been incubated for 90–120 min (Fig. 5D), to CA1 pyramidal neurons of 2–4 month-old wild-type mice in vivo, which robustly induced neuronal hyperactivation (Fig. 5, E and J), in contrast to the observed ineffectiveness of the freshly prepared monomer solution (Fig. 4). Likewise, ‘aged’ A $\beta$  application also caused neuronal hyperactivation in hippocampal slices, both at concentrations of 1 and 100  $\mu$ M monomer equivalent (Fig. S10, A to D).

Given that the ThT-fluorescence assay indicates that the A $\beta$ -anticalin prevents the formation of A $\beta$  fibrils (Fig. 5B), we asked whether the A $\beta$ -anticalin could also prevent the formation of toxic soluble A $\beta$  dimers and oligomers. Thus, we next administered the solution of A $\beta$  monomers, which had been incubated in vitro with a stoichiometric concentration (1:1) of the A $\beta$ -anticalin for 90–120 min

(Fig. 5F). The application of this solution in vivo did not induce neuronal hyperactivation (Fig. 5, G and K), demonstrating, first, that toxic A $\beta$  dimers or oligomers had not formed and, second, that anticalin-bound A $\beta$  monomers do not induce neuronal hyperactivation (Fig. 5L). Likewise, the application of this solution did not change the neuronal activity levels in bicuculline-treated hippocampal slices (Fig. S8, E and F).

Next, we asked whether the neutralizing effect of the A $\beta$ -anticalin might at least partially be mediated by the disintegration of neurotoxic A $\beta$  aggregates. When we applied the mixture of ‘aged’ A $\beta$  and A $\beta$ -anticalin (Fig. 5C) in the hippocampal CA1 region in vivo, it induced neuronal hyperactivation (Fig. 5, I and M), which was indiscernible from that caused by the A $\beta$  oligomers alone (Fig. 5N). In addition to the increased number of Ca<sup>2+</sup>-transients, we analyzed the AUC for the respective Ca<sup>2+</sup>-signals (Fig. S11). We found that the application of aged A $\beta$  alone or together with the A $\beta$ -anticalin reliably increased the AUC by a similar percentage. In contrast, the application of freshly prepared A $\beta$  monomers alone or incubated with the A $\beta$ -anticalin had no effect. In line with this, in the SEC analysis of the mixture between aged A $\beta$  and the A $\beta$ -anticalin, we found a slight shift to a lower elution volume (in line with larger size by  $\sim 2.7$  kDa) as well as a broadening of the peak compared to the anticalin protein alone (Fig. S12). This indicates the binding of residual A $\beta$  monomers but not of larger oligomers or aggregates to the A $\beta$ -anticalin.

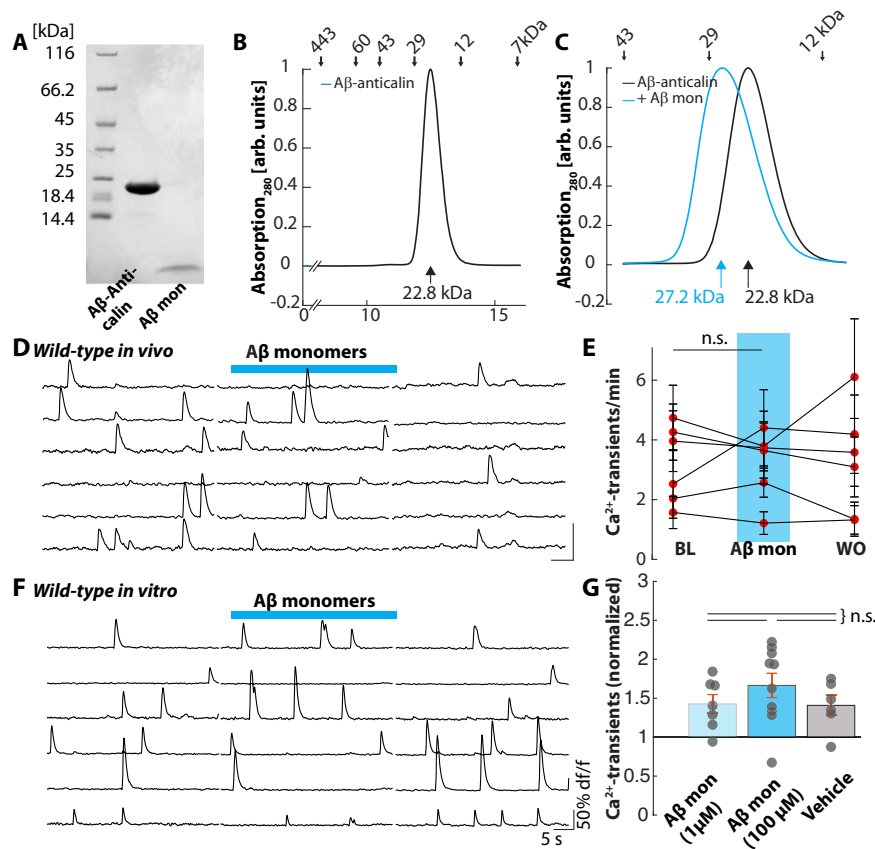


**Fig. 4 | A $\beta$ -anticalin binds inactive A $\beta$  monomers.** **A** Coomassie-stained SDS/PAGE depicting the size of A $\beta$ -anticalin (21.3 kDa) and A $\beta$  monomer (4.4 kDa). The experiment was repeated twice. **B** Size exclusion chromatography (SEC) of the A $\beta$ -anticalin shows a peak at an elution volume of 12.48 ml, corresponding to an apparent molar weight of 22.7 kDa. **C** SEC of freshly prepared A $\beta$ (1-40) monomers (calculated molar weight: 4430 Da) in combination with A $\beta$ -anticalin demonstrate a shift of the peak from 12.48 to 12.07 ml, suggesting binding of the 4.4 kDa-peptide by the anticalin. **D** Representative Ca<sup>2+</sup>-traces recorded from six hippocampal CA1 neurons of a wild-type mouse under baseline conditions, during the application of A $\beta$  monomers (10  $\mu$ M, applied 5 min after preparation of the solution) and after a washout period of 5 min. **E** Summary data of the experiments in (D) from  $N = 6$  mice. Each dot represents the mean number of Ca<sup>2+</sup>-transients per minute, for all

observed neurons in one mouse under baseline conditions (BL), during the application of A $\beta$  monomers (A $\beta$  mon) and under washout conditions (WO). **F** Ca<sup>2+</sup>-transients from six representative CA1 pyramidal neurons in a bicuculline-treated hippocampal slice from a wild-type mouse under baseline conditions (left), during the application of A $\beta$ (1-40) monomers (1  $\mu$ M, applied 5 min after preparation of the aqueous solution) through a patch pipette (middle) and after washout for 5 min (right). **G** Number of Ca<sup>2+</sup>-transients during the application of 1  $\mu$ M A $\beta$  monomers ( $N = 6$  slices), 100  $\mu$ M A $\beta$  monomers ( $N = 10$ ) or ACSF as vehicle solution ( $N = 6$ ), normalized to the respective mean baseline activity. n.s. not significant. Source data for Fig. 4G are provided as a Source Data file. Error bars depict SEM. Two-sided Wilcoxon signed-rank test (E) or Kruskal-Wallis test with Dunn-Sidak post-hoc comparison (G).

In light of the apparent lack of binding to aggregated A $\beta$ -species, it is important to ask whether A $\beta$ -anticalin treatment can also be effective in older *APP23xPS45* mice with a large number of plaques (Fig. S13A). While old *APP23xPS45* mice also had a high percentage of hyperactive neurons (Fig. S13B), which was similar to that of young animals, the application of the A $\beta$ -anticalin only marginally reduced neuronal activity levels in 7–8 month-old plaque-bearing AD animals (Fig. S13, C and D). Likewise, the application of the  $\gamma$ -secretase inhibitor had a markedly smaller effect on preventing neuronal hyperactivity in the aged AD mice compared to young mice (Fig. S10 E, F).

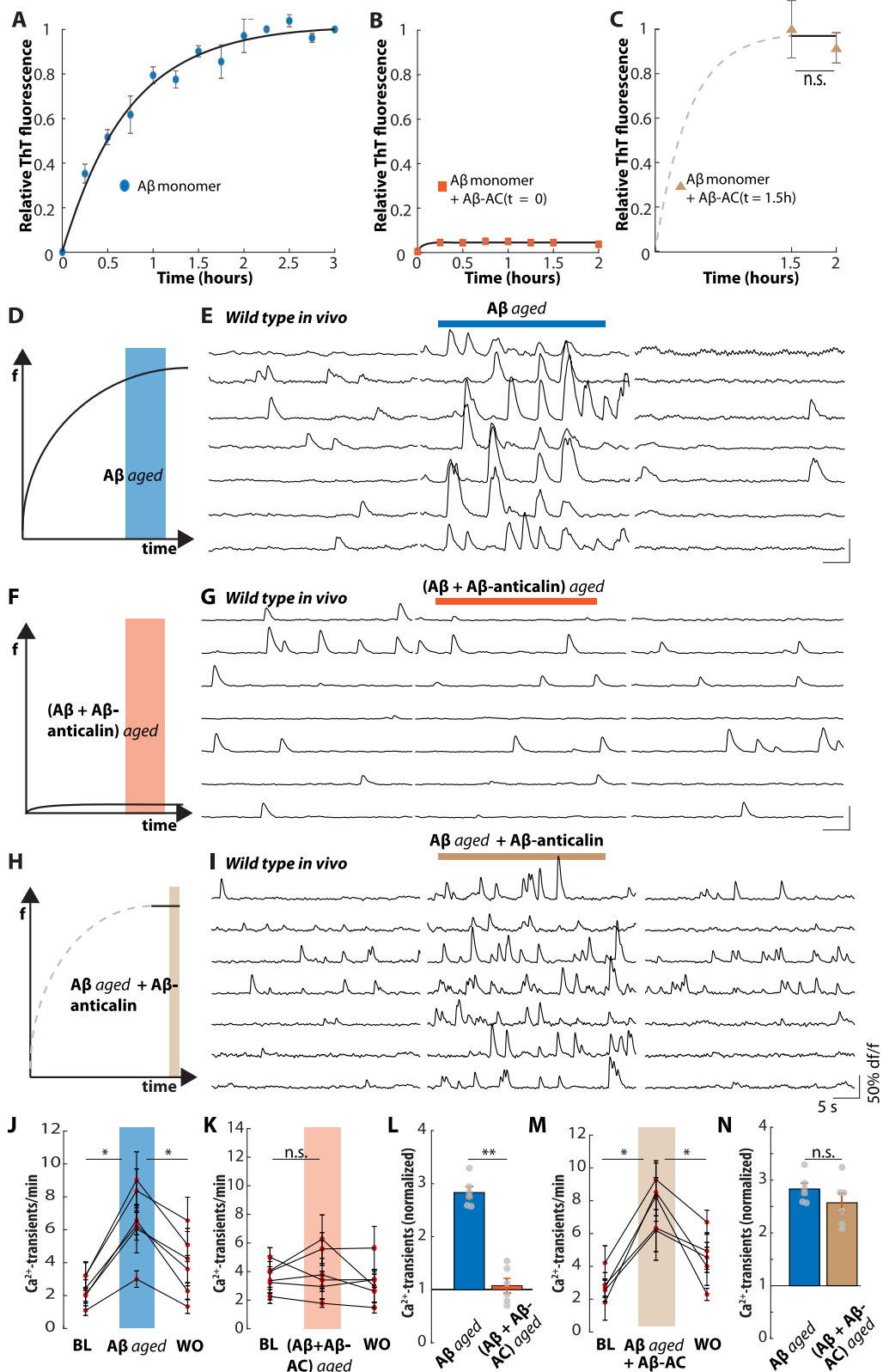
Finally, we asked whether the A $\beta$ -anticalin dependent prevention of A $\beta$  aggregation also prevented perisynaptic glutamate accumulation. To this end, we expressed the fluorescent glutamate indicator SF-iGluSnFR A184S in the CA1 region of wild-type mice (Fig. 6A, B) and synaptically induced extracellular glutamate transients (Fig. 6C, left) by electric stimulation of the Schaffer collaterals. The application of ‘aged’ A $\beta$ -solution (Fig. 5A) caused a robust increase in the synaptically evoked glutamate transients (Fig. 6C, middle), which was reversible after a washout of 5–10 min (Fig. 6C, right). These results were similar to previous results with [A $\beta$ S26C]<sub>2</sub><sup>18</sup>. In contrast, the application of a similarly ‘aged’ solution of an A $\beta$ (40-1) peptide with reverse sequence,

which does not form aggregates<sup>43</sup>, did not affect synaptically evoked glutamate transients (Fig. 6D). In a parallel approach, injection of A $\beta$ (1-40) solution incubated with the A $\beta$ -anticalin (Fig. 5B), putatively containing bound A $\beta$  monomers, did not enhance synaptically evoked glutamate transients (Fig. 6, E and F). Together, these data demonstrate that preventing the formation of toxic A $\beta$  oligomers or aggregates also prevents the synaptic dysfunction underlying A $\beta$ -induced neuronal hyperactivity.

## Discussion

In this study, we demonstrate that scavenging A $\beta$  monomers by an A $\beta$ -anticalin can restore normal neuronal activity levels in mouse models of AD and provide mechanistic evidence for its rescue action. Under disease conditions, naturally secreted A $\beta$  monomers, which are pathologically inactive, rapidly form toxic dimers and oligomers that cause neuronal hyperactivity in vivo. However, adding the A $\beta$ -anticalin at the beginning of the aggregation cascade scavenges A $\beta$  monomers, thereby preventing the formation of toxic aggregates. In consequence, neuronal activity levels remain unaltered (Fig. 6G).

Hippocampal hyperactivity is an early neuronal dysfunction of AD in mice and humans, precedes plaque deposition as well as overt brain



atrophy<sup>17,44</sup>, and is associated with the break-down of circuits and impaired cognition<sup>45,46</sup>. Moreover, studies in mice and humans demonstrated that the effective suppression of neuronal hyperactivity can improve or even restore cognitive function<sup>20,47</sup>. Neuronal hyperactivity can be prevented or reduced in mouse models by blocking Aβ secretion<sup>10,20</sup>, but previous attempts at scavenging Aβ using parenteral application of mAbs have even exacerbated neuronal dysfunction<sup>6</sup>.

Consequently, our findings that the direct intracerebral application of the Aβ-anticalin and, to a certain degree, also Solanezumab can restore normal neuronal activity, demonstrate the feasibility of such approaches.

Moreover, we provide direct evidence using fluorescent glutamate indicators that scavenging of Aβ by the Aβ-anticalin prevents extracellular glutamate accumulation, a prominent feature of AD,

**Fig. 5 | Prevention of the formation of toxic aggregates of the A $\beta$ -anticalin.** **A** In vitro aggregation assay of synthetic A $\beta$ (1-40) monomers. Average ( $n = 3$  experiments) and SEM are shown. The values were normalized to the maximum fluorescence. **B** same as (A) for samples taken from the A $\beta$  aggregation assay in the presence of the A $\beta$ -anticalin (A $\beta$ -AC). **C** Same as (B) after aggregation for 90 min and following the addition of the A $\beta$ -anticalin. **D** Scheme depicting the aggregation curve of A $\beta$ (1-40) monomers in the ThT assay. **f**, fluorescence. **E** Representative Ca $^{2+}$ -traces recorded from seven hippocampal CA1 neurons of a wild-type mouse during baseline, during the application of putative A $\beta$  oligomers (10  $\mu$ M monomer equivalent) and after washout. **F** Scheme depicting the ThT-aggregation assay in the presence of A $\beta$  and the A $\beta$ -anticalin (10  $\mu$ M, respectively). **G** Same as (E) for the application of putative protein-bound A $\beta$  monomers. **H** Scheme depicting the aggregation of A $\beta$  monomers alone for 90 min and after the addition of A $\beta$ -

anticalin. **I** Same as (E) for the application of 'aged' A $\beta$  (10  $\mu$ M monomer equivalent), incubated with 10  $\mu$ M A $\beta$ -anticalin for a further 30 min. **J** Summary data of the experiments in (E) from  $N = 6$  mice under baseline conditions (BL), during the application of 'aged' A $\beta$  and after washout (WO). **K** same as (J) for the experiment in (G) and the application of A $\beta$ /A $\beta$ -anticalin. **L** Number of Ca $^{2+}$ -transients during the application of 'aged' A $\beta$  ( $N = 6$ ) or A $\beta$ /A $\beta$ -anticalin ( $N = 6$ ), normalized to the respective mean baseline. **M** same as (J) for the experiment in (I) and the application of 'aged' A $\beta$ , incubated with A $\beta$ -anticalin. **N** Number of Ca $^{2+}$ -transients during the application of 'aged' A $\beta$  ( $N = 6$ ) or 'aged' A $\beta$ , incubated with A $\beta$ -anticalin ( $N = 6$ ), normalized to the respective mean baseline activity. Data in 5C and 5J–N are presented as mean  $\pm$  SEM. Source data for Fig. 5L and N are provided as a Source Data file. Data in n.s. not significant, \* $p < 0.05$ , \*\* $p < 0.005$ , Two-sided Wilcoxon signed-rank test (J, K, M), Two-Wilcoxon rank sum test (C, L, N).

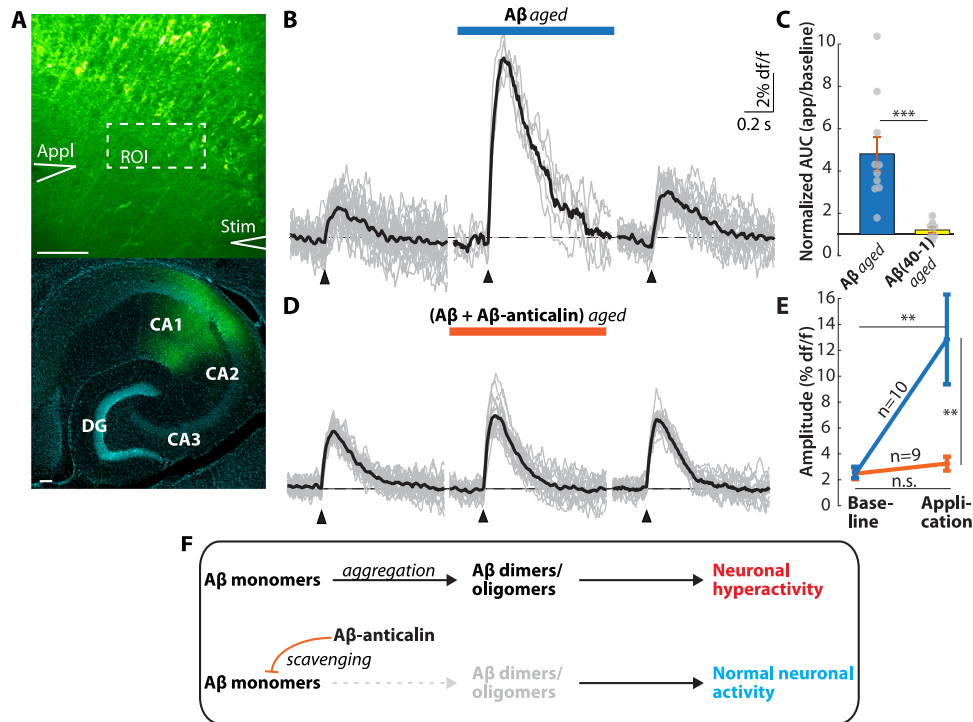


**Fig. 6 | The A $\beta$ -anticalin prevents A $\beta$ -dependent synaptic dysfunctions.** **A Top:** representative two-photon image of the SF-iGluSnFrA184S-expressing CA1 region of a wild-type mouse. The location of the application (*Appl*) and the stimulation (*Stim*) pipette, as well as the region of interest (ROI) from which glutamate transients were recorded, are outlined in white. **Bottom:** post-hoc confocal image of the SF-iGluSnFr-expressing neurons in CA1 (green) and DAPI counterstaining (cyan). DG: dentate gyrus, CA: cornu ammonis. Scale bars: 100  $\mu$ m. **B** Individual synaptically evoked glutamate transients (gray) and average (black) from one slice during baseline conditions (left), during the application of 'aged' A $\beta$  (50  $\mu$ M monomer equivalent, incubated for 20 min in ACSF; middle) and after washout (right). **C** Area under the curve (AUC) of the evoked glutamate transients during the application of 'aged' A $\beta$ (1-40) ( $N = 10$  slices) or 'aged' reverse A $\beta$ (40-1) ( $N = 9$ ), normalized to the respective AUC registered under baseline conditions. Data are presented as mean

values  $\pm$  SEM. **D** Same as (C) for the application of A $\beta$  + A $\beta$ -anticalin (50  $\mu$ M A $\beta$  monomer equivalent, incubated in ACSF containing 50  $\mu$ M of the A $\beta$ -anticalin for 20 min). **E** Comparison of the amplitudes of glutamate transients before (left) and during (right) the application of 50  $\mu$ M equivalent A $\beta$  monomer, incubated for 20 min without (blue) or with (orange) A $\beta$ -anticalin (mean  $\pm$  SEM). **F** Scheme depicting the mechanism of action of the A $\beta$ -anticalin. Under disease conditions, nascent A $\beta$  monomers rapidly aggregate into toxic dimers and oligomers, which cause neuronal hyperactivity (top). Scavenging these monomers by the A $\beta$ -anticalin disrupts the formation of toxic dimers/oligomers, thus preventing neuronal hyperactivation (bottom). Source data for Fig. 6C are provided as a Source Data file. n.s. not significant, \*\* $p < 0.005$ , \*\*\* $p < 0.001$ . Two-sided Wilcoxon rank sum test (C, E across groups); Wilcoxon signed-rank test (E, baseline vs. application).

which is associated with impaired synaptic integrity and plasticity as well as a mechanism of neuronal hyperactivity<sup>18,31,33,48</sup>. Our glutamate imaging data in hippocampal slices demonstrates that the extent of the perisynaptic glutamate accumulation is correlated with the amount of synaptic stimulation. This is in line with our previous findings that A $\beta$ -dependent neuronal hyperactivation requires ongoing synaptic input<sup>18</sup>. Our data provide a mechanistic explanation for the reduced neuronal hyperactivity observed in our *in vivo* experiments.

In line with previous reports<sup>18,38,39</sup>, we found that A $\beta$  monomers are pathologically inert. Thus, solutions containing the freshly

prepared A $\beta$  monomers only or A $\beta$  monomers stably bound by the A $\beta$ -anticalin failed to induce neuronal hyperactivity both *in vivo* and *in vitro* and, furthermore, did not lead to extracellular glutamate accumulation. On the contrary, a solution of aggregated, i.e. 'aged', A $\beta$  including dimers and oligomers, potentially perturbed neuronal function. These observations reinforce previous findings that such oligomers are the most toxic species of A $\beta$ <sup>18,36,49,50</sup>.

In light of this, the rapidity of the hyperactivity-reducing effect of the A $\beta$ -anticalin application *in vivo* is remarkable because the brains of APP23xPS45 mice already contain elevated levels of oligomeric or



aggregated A $\beta$ <sup>20</sup>. Thus, our data suggest that neuronal dysfunction in early AD largely depends on the continuous de novo release of (nascent) A $\beta$  monomers, which immediately start forming toxic oligomers or aggregates, rather than a stable pool of such A $\beta$  species. In consequence, it is likely that existing oligomers are quickly rendered innocuous in vivo, either by clearance from the brain or by the formation of larger, less toxic aggregates<sup>50</sup>. Additional evidence for this hypothesis comes from a parallel experiment with application of a  $\gamma$ -secretase inhibitor, which had a very similar effect as the A $\beta$ -anticalin in our in vivo hyperactivity assay. In line with this, previous studies have shown that systemic  $\gamma$ -secretase inhibitor treatment prevents the release of A $\beta$  peptides into the extracellular space<sup>51</sup>, leads to a rapid decrease of total<sup>30,52</sup> and oligomeric<sup>10</sup> A $\beta$  levels in mouse models of  $\beta$ -amyloidosis and, concomitantly, normalized neuronal activity<sup>10</sup>. While previous findings did not exclude that oligomers can form intracellularly before they are released<sup>53–55</sup>, based on the efficacy of the A $\beta$ -anticalin in *APP23xPS45* mice, it is unlikely that such released oligomers reach sufficiently high concentrations to cause neuronal dysfunction in vivo.

Taken together, our data indicate that, in young AD mice, monomer scavenging by the A $\beta$ -anticalin or Solanezumab can prevent A $\beta$ -induced neurotoxic effects by scavenging the monomeric peptide and interfering with its aggregation without the need or ability to dissolve preexisting oligomers.

In older, plaque-bearing *APP23xPS45* mice, on the other hand, scavenging monomers alone was not sufficient to reduce neuronal hyperactivity, possibly because oligomers are not only formed from nascent A $\beta$  monomers in these aged animals but can also be released from larger aggregates<sup>50,56</sup>. However, our data are compatible with the possibility that A $\beta$ -anticalin treatment may be a valuable addition to therapies aiming at the removal of large aggregates.

The current study demonstrates that A $\beta$ -anticalin dependent A $\beta$  monomer scavenging can repair neuronal and synaptic dysfunctions in mouse models of AD in vivo. However, the main limitation of our approach is that, by the direct and acute injection of the A $\beta$ -anticalin in a defined small brain area, we were only able to investigate local short-term effects of the application. In consequence, more work is needed to clarify whether A $\beta$ -anticalin application may also constitute a promising therapeutic strategy and can mitigate plaque pathology and cognitive decline longitudinally. Their small size and efficacy at relatively low concentrations, and higher efficacy over the antibody Solanezumab in our assay, together with a lack of immunological effector functions as well as interactions with plasma proteins<sup>24</sup>, make the A $\beta$ -anticalin a potential candidate drug for further investigation as a possible therapeutic entity for the preventive treatment of early AD.

## Methods

All experimental procedures were performed in compliance with all relevant ethical regulations and were explicitly approved by the government of upper Bavaria (animal protocol numbers: 55.2-1-54-25323-11, 55.2.1.54-2532-66-13, ROB-55.2-2532.Vet\_02-16-155, ROB-55.2-2532.Vet\_02-21-121).

## Animal models

In vivo experiments were performed with 2–4 month-old (young group) and 7–9 month-old (old group) C57 Bl/6N wild-type mice of both sexes or with age-matched female *APP23xPS45* mice expressing the APP Swedish mutation (670/671) and the G384A mutation in the presenilin 1 (PS1) gene under the Thy-1 promoter<sup>14</sup>. Additionally, we used 4–8 month-old *APP23* mice of both sexes<sup>57</sup>. All mice were housed in standard mouse cages under a 12-h dark/12-h light cycle and constant temperature ( $\sim 25^\circ\text{C}$ ) and humidity ( $\sim 55\%$ ). Food and water were provided ad libitum.

## Surgery

In vivo two-photon imaging was performed in line with previous reports<sup>10,18</sup>. Mice were initially anesthetized with isoflurane (2% vol/vol in pure O<sub>2</sub>). The scalp was partially removed and a custom-made plastic recording chamber with a central opening was attached to the skull using dental cement. The skull was thinned with a dental drill (Meisinger, Neuss, Germany) in a circle with a diameter of approximately 2 mm with the center on top of the hippocampal CA1 region (AP  $-2.75$ , ML 3.5) and the recording chamber was filled with artificial cerebrospinal fluid (ACSF; 125 mM NaCl, 4.5 mM KCl, 26 mM NaHCO<sub>3</sub>, 1.25 mM NaH<sub>2</sub>PO<sub>4</sub>, 2 mM CaCl<sub>2</sub>, 1 mM MgCl<sub>2</sub>, 20 mM glucose, pH 7.4 when bubbled with carbogen gas), which had been warmed to 37 °C. The bone was carefully removed with a thin cannula to open a cranial window directly above the imaged region. The dura and cortical tissue covering the hippocampus were removed by suction. After this, multi-cell bolus loading was performed with the organic Ca<sup>2+</sup>-indicator Cal-520 AM<sup>58</sup>, injected through a glass patch pipette 200  $\mu\text{m}$  underneath the hippocampal surface. After the surgery, the concentration of Isoflurane was reduced to 0.8–1.0% vol/vol for imaging.

## Anticalin preparation and antibodies

The A $\beta$ -specific Anticalin was prepared via soluble cytoplasmic expression in 2 L shake flask cultures of *E. coli* Origami B<sup>59</sup>. Wild-type Lcn2 was periplasmatically expressed in *E. coli* W3310<sup>60,61</sup>. Both proteins were purified by His<sub>6</sub>-tag affinity chromatography<sup>62</sup> and SEC on a Superdex 75 HR 26/60 column (GE Healthcare, Munich, Germany) using HEPES-Ringer (135 mM NaCl, 5 mM KCl, 2 mM CaCl<sub>2</sub>, 1 mM MgCl<sub>2</sub>, 10 mM HEPES, 20 mM Glucose, pH 4.7) or phosphate-buffered saline (PBS; 4 mM KH<sub>2</sub>PO<sub>4</sub>, 16 mM Na<sub>2</sub>HPO<sub>4</sub>, 115 mM NaCl, pH 7.4). Protein purity was checked by SDS/PAGE<sup>63</sup> and ESI mass spectrometry on an maXis instrument (Bruker Daltronics, Bremen, Germany) in the positive ion mode. Endotoxins were removed using NoEndo™ HC (High Capacity) Spin Columns (Protein Ark, Rotherham, UK) and residual pyrogen levels were analyzed using the Endosafe-PTS™ (Charles River Laboratories, Wilmington, USA) resulting in  $< 5$  EU/mL. Protein concentration was determined via absorption at 280 nm using molar absorption coefficients calculated with the ExpASY ProtParam tool<sup>64</sup>.

The IgG Solanezumab biosimilar antibody was obtained from Antibodies-online (Cat.# ABIN7487922, CAS 955085-14-0), the Goat anti-Rabbit IgG unconjugated control antibody was purchased from Invitrogen (Cat.# A27033). Proteins were stored at  $-20^\circ\text{C}$  and diluted to the end concentration of 1  $\mu\text{M}$  in ACSF or HEPES-Ringer immediately before the experiment.

## A $\beta$ peptides

A $\beta$ (1-40) and A $\beta$ (40-1), the latter with a reverse amino acid sequence, were obtained from Bachem Pharmaceuticals (Bubendorf, Germany). The A $\beta$ (1-40)/S26C dimer [A $\beta$ S26C]<sub>2</sub> was from jpt (Berlin, Germany). All peptides were dissolved in DMSO and stored frozen. Immediately before the experiments, the peptides were thawed and diluted in ACSF or HEPES-Ringer or in Ringer solution containing an equimolar amount of the A $\beta$ -anticalin. The solution was pressure applied through a glass patch pipette either immediately or incubated at room temperature (25 °C) for the indicated time and centrifuged at  $-4400$  g for 5 min to remove insoluble aggregates before application.

## Hippocampal slice preparation

Mice were anesthetized and decapitated. The brain was surgically removed and submerged in ice-cold slicing solution (24.7 mM glucose, 2.48 mM KCl, 65.47 mM NaCl, 25.98 mM NaHCO<sub>3</sub>, 105 mM sucrose, 0.5 mM CaCl<sub>2</sub>, 7 mM MgCl<sub>2</sub>, 1.25 mM NaH<sub>2</sub>PO<sub>4</sub>, 1.7 mM ascorbic acid) with an osmolarity of 290–300 mOsm and a pH of 7.4, which was stabilized by bubbling with carbogen gas. Horizontal slices (300  $\mu\text{m}$ )

were cut using a vibratome. These were allowed to recover at room temperature for at least one hour in a recovery solution containing 2 mM CaCl<sub>2</sub>, 12.5 mM glucose, 2.5 mM KCl, 2 mM MgCl<sub>2</sub>, 119 mM NaCl, 26 mM NaHCO<sub>3</sub>, 1.25 mM NaH<sub>2</sub>PO<sub>4</sub>, 2 mM thiourea (Sigma, St. Louis, USA), 5 mM Na-ascorbate (Sigma), 3 mM Na-pyruvate (Sigma), and 1 mM glutathione monoethyl ester. The pH was adjusted to 7.4 with HCl, and the osmolarity was 290 mOsm. Before the imaging experiment, the Schaffer collaterals were cut and the slices were transferred into the recording setup and superfused with warmed (37 °C) ACSF. To induce in vivo-like ongoing baseline activity in the hippocampal slices, 100 μM bicuculline was added to the ACSF and the potassium concentration was slowly increased to 5.5–6.5 mM (for a detailed description, see<sup>18</sup>). For calcium imaging experiments, bolus loading of Cal-520 AM was performed as described above.

### Two-photon Ca<sup>2+</sup>-imaging and application of Aβ and/or anticalins

In vivo and in vitro two-photon Ca<sup>2+</sup> imaging was performed in the same custom-made multi-photon recording setup based on an upright microscope (Olympus, Shinjuku, Japan)<sup>18</sup>. Excitation light was provided by a tunable Ti:sapphire laser at a wavelength of 920 nm (Coherent, Santa Clara, USA). Fluorescence images were collected using a resonant galvo mirror scanner operating at 8 or 12 kHz (GSI group, Bedford, USA) as well as a 40 × 0.8 NA objective (Nikon, Tokyo, Japan). Full frames were acquired at 40 Hz.

After surgery or slice preparation and Cal-520 AM bolus loading (see above), spontaneous Ca<sup>2+</sup> transients were recorded from the pyramidal layer of hippocampal CA1. For the injection of Aβ and/or anticalins a glass patch pipette (tip resistance 1–2 MΩ) was filled with approximately 5 μl of the peptide/protein application solution (see above) and the tip was positioned in the pyramidal layer of the hippocampal CA1 region under visual control (about 150 μm under the hippocampal surface in vivo or 50 μm below the slice surface in vitro). The pressure was carefully applied using a picospritzer II (Parker, Cleveland, USA) until a slight tissue displacement in front of the tip indicated fluid ejection (typically around 20 mBar). In some experiments, this was further validated by adding 5 μM Alexa 594 dye (Thermo Fischer, Waltham, USA) to the pipette solution. The pressure was stopped after 30–60 s. The same field of view was monitored during baseline, pressure application, and washout conditions.

### Virus injection and glutamate imaging

AAV2/1.hSynapsin.iGluSnFR A184S<sup>65</sup> was a gift from Loren Looger (HHMI/Janelia), AAV1.hSyn.FLEX.iGluSnFR3.v857.PDGFR.codonopt and AAV1.hSyn.Cre.WPRE.hGH were purchased from Addgene (Cat#175180-AAV1 and Cat#105553-AAV1). Virus injection and two-photon population glutamate imaging was performed in a similar fashion as previous reports<sup>18,35</sup>. Thus, 500 nl of AAV2/1.hSynapsin.iGluSnFR A184S (2.4 × 10<sup>12</sup> gc/ml) or AAV1.hSyn.FLEX.iGluSnFR3.v857.PDGFR.codonopt (3.5 × 10<sup>12</sup> gc/ml) and AAV1.hSyn.Cre.WPRE.hGH (7.3 × 10<sup>11</sup> gc/ml) were injected into the hippocampal CA1 region (AP -2.75, ML 3.5 and DV 2–3 mm) of isoflurane-anesthetized 4–6 week-old mice by slow (10–20 nl/min) pressure injection from a glass pipette. After the retraction of the injection pipette, mice were transferred back to their home cage, where 2–3 weeks were allowed for viral expression.

After that, hippocampal slices were prepared as described further above or, for the experiments in Fig. 6, according to the Optimized N-Methyl-D-glucamine Protective Recovery Method<sup>66</sup> with sodium spiking at 34 °C. Glutamate two-photon imaging was performed in the stratum radiatum of the hippocampal CA1 area under illumination at 920 nm with a framerate of 120 Hz for iGluSnFR.A184S and 200 Hz for iGluSnFR3. For experiments with the iGluSnFR3 construct a deformable mirror (DM97-15, Alpao, Montbonnot, France) was introduced in the light path and different Zernicke modes were applied to optimize

image resolution and contrast for each experiment. Synaptic glutamate release was achieved by electrical stimulation of the Schaffer collaterals in CA1. In Fig. 6, single action potentials were evoked with a glass pipette (30–40 V, 100 μs). In Fig. 2, trains of action potentials were evoked by a concentric bipolar electrode (FHC, Bowdoin, USA, Cat.# 30201) at 12–14 V, 100 μs pulse duration and 20 ms interpulse interval. Aβ peptide and/or anticalin were pressure applied in the field of view through a second glass pipette.

### Image analysis

Offline image analysis was performed as described previously<sup>67</sup>. Fluorescence traces were extracted from the imaging data using custom-written software based on LabVIEW. In Ca<sup>2+</sup>-imaging experiments, neurons were visually identified and regions of interest (ROIs) were drawn around their somata. Astrocytes were excluded from the analysis due to their morphology and their high fluorescence levels<sup>68</sup>. In glutamate imaging, a region of interest (ROI) was drawn over the full imaging frame. The fluorescence of each ROI over time was extracted, low-pass filtered to 10 Hz (Ca<sup>2+</sup>) or 40 Hz (glutamate) and normalized to the baseline as  $df/f = (f(t) - f_0)/f_0$ , where  $f_0$  was set at the 10<sup>th</sup> percentile of the entire trace in Ca<sup>2+</sup>-imaging or at the mean of the pre-stimulus interval in glutamate imaging experiments. Fluorescence changes with peak amplitudes three times larger than the standard deviation of the baseline were accepted as neuronal calcium or extracellular glutamate transients. To calculate the area under the curve (AUC) in Fig. S11, a time-dependent baseline was determined for each cell<sup>67</sup> to prevent confounding effects by slow drifts, especially during application periods. The AUC was calculated individually for each neuron using the trapezoidal rule during 40 s of baseline and the first 40 s of the respective application. For glutamate transients, the AUC was calculated using the trapezoidal rule within 0.5 s after stimulation.

### Measurement of binding activity using surface plasmon resonance (SPR)

Kinetic affinity data of the Aβ-anticalin (HIGA) and the recombinant wild-type lipocalin 2 (Lcn2) were measured at 25 °C on a BIAcore 2000 system (BIAcore, Uppsala, Sweden) with immobilized Aβ(1-40) (Bachem) according to a published procedure<sup>23</sup> using HBS-T (20 mM HEPES/NaOH pH 7.5, 150 mM NaCl and 0.005% v/v Tween20) as running buffer. ~350 RU of Aβ(1-40) was covalently immobilized on a CMS chip (GE Healthcare) using amine coupling chemistry in 10 mM sodium acetate buffer pH 5. Dilution series of the purified lipocalin proteins were applied at a flow rate of 30 μl/min. The data were double-referenced by subtraction of the corresponding signals measured for the control channel and of the average of three buffer injections<sup>69</sup>. Kinetic parameters were determined by global fitting of single-cycle kinetics with BIAevaluation software v 4.1 using the Langmuir 1:1 binding model. The equilibrium dissociation constants were calculated as  $K_D = k_{off}/k_{on}$  and the statistical error was estimated as previously described<sup>70</sup>.

### Analytical size exclusion chromatography

2.5 μl of a 5 mM Aβ(1-40) monomer solution in DMSO was mixed with 247.5 μl of 50 μM Aβ-anticalin solution in HEPES-Ringer, resulting in a 1:1 molar ratio of Aβ-anticalin to Aβ. In a control experiment, only the buffer without the Aβ-anticalin was used. 100 μL of the sample was cleared from aggregates by centrifugation in a bench top centrifuge at ~20,000 g (5 min, room temperature) and directly applied to SEC. The remaining sample was incubated for 90 min at room temperature, again followed by SEC after centrifugation. The chromatography was performed on a 24 ml Superdex 75 10/300 GL column (GE Healthcare) using HEPES-Ringer buffer pH 7.4 at a flow rate of 0.5 ml/min. The column was calibrated with the following protein standards (Sigma-Aldrich): alcohol dehydrogenase (ADH, 150 kDa) bovine serum

albumin (BSA, 66 kDa), ovalbumin (43 kDa), carbonic anhydrase (CA, 29 kDa), cytochrome c (Cyt c, 12.4 kDa) and aprotinin (Ap, 6.5 kDa). Blue dextran was applied to determine the void volume of the column. Based on the peak elution volumes, the partition coefficients ( $K_{av}$ ) were calculated and used to interpolate the apparent molecular masses of the A $\beta$ /anticalin mixtures.

### ThioflavinT fluorescence assay

The ThT Assay was carried out according to previously published procedure<sup>23</sup>. A $\beta$ (1-40) was lyophilized and dissolved in 1,1,1,3,3,3-hexafluoro-2-propanol (HFIP; Sigma–Aldrich) at a concentration of 5 mg/ml. Following the evaporation of HFIP in the fume hood for 12 h, the dried A $\beta$ (1-40) was dissolved in 250  $\mu$ l ice-cold H<sub>2</sub>O. After sonication for 15 min at 4 °C (Sonorex, Bandelin, Berlin, Germany), the peptide solution was sterile-filtered with a Costar Spin-X centrifuge tube filter, 0.45  $\mu$ m pore size cellulose acetate membrane (Corning Life Sciences, Kaiserslautern, Germany). The freshly prepared solution of monomeric A $\beta$ (1-40) was immediately used for the aggregation assay by mixing the 2 mg/ml (462  $\mu$ M) A $\beta$ (1-40) monomer solution with either 250  $\mu$ l A $\beta$ -anticalin solution in PBS at a 1:1 molar ratio or PBS alone. Aggregation reactions were performed in triplicates at 25 °C or 37 °C in 2 ml DNA LoBind Tubes (Eppendorf, Hamburg, Germany) with stirring at 500 rpm using a 5 mm magnetic bar. For fluorescence measurements, 20  $\mu$ l samples were removed at distinct time points and mixed with 180  $\mu$ l of a 55.6  $\mu$ M solution of Thioflavin T (ThT) (Sigma–Aldrich) in 0.5  $\times$  PBS and analyzed in a FluoroMax-3 spectrofluorometer (HORIBA Jobin Yvon, Bensheim, Germany) using an excitation wavelength of 450 nm and an emission wavelength of 482 nm. The integration time was set to 20 s with a slit width of 2 nm. Measured fluorescence intensities were set to zero for  $t = 0$  and the asymptotic value of the fluorescence intensity of aggregated A $\beta$ (1-40) in 0.5  $\times$  PBS was set to 100%.

### Confocal plaque imaging

For plaque staining, mice were injected intraperitoneally with Methoxy-X04 (1.7 mg/kg body weight). After 18 h, the mice were perfused intracardially with 4% PFA and the brains were post-fixed overnight<sup>71</sup>. The next day, coronal sections were prepared and NeuroTrace deep red counterstaining was performed<sup>72</sup>. Slices were mounted in a confocal microscope (Olympus) and images were taken using a 4X air immersion objective and stitched together.

### Statistics and Reproducibility

For the comparison of two groups, we used two-tailed Wilcoxon signed-rank or rank sum tests. For the comparison of multiple groups, we used a Kruskal–Wallis test with Dunn–Sidak post-hoc comparison or a Kolmogorov–Smirnov-Test. The sigmoidal curve in Fig. S4B was created by non-linear regression, using SEM data weight, according to the Equation of Mass Law. Details on the exact statistical test used as well as the number of subjects and samples are included in the respective figure legends. N-numbers were equal to comparable two-photon in vivo imaging studies and explicitly experiments from our group and others investigating neuronal dysfunctions in AD<sup>10,12,14,18,33</sup>. No statistical method was used to predetermine sample size. When comparing the effects of the application of different proteins/peptides and controls, animals were randomized. Blinding was not possible, because, due to the neuronal hyperactivity in AD mice, their genotype would be immediately apparent to the experimenter.

### Reporting summary

Further information on research design is available in the Nature Portfolio Reporting Summary linked to this article.

### Data availability

The crystal structure of the A $\beta$ -anticalin bound to A $\beta$  1-40<sup>24</sup> is available at the RCSB protein data bank under accession code 4MVL. The

remaining data generated in this study are provided in the Supplementary Information/Source Data file. Raw data will be provided upon reasonable request to the corresponding authors. Source data are provided with this paper.

### References

1. Selkoe, D. J. & Hardy, J. The amyloid hypothesis of Alzheimer's disease at 25 years. *EMBO Mol Med* **8**, 595–608 (2016).
2. Hong, S. et al. Complement and microglia mediate early synapse loss in Alzheimer mouse models. *Science* **352**, 712–716 (2016).
3. Jin, M. et al. Soluble amyloid beta-protein dimers isolated from Alzheimer cortex directly induce Tau hyperphosphorylation and neuritic degeneration. *Proc Natl Acad Sci USA* **108**, 5819–5824 (2011).
4. Kadowaki, H. et al. Amyloid  $\beta$  induces neuronal cell death through ROS-mediated ASK1 activation. *Cell Death Differ* **12**, 19 (2004).
5. Panza, F., Lozupone, M., Logroscino, G. & Imbimbo, B. P. A critical appraisal of amyloid-beta-targeting therapies for Alzheimer disease. *Nat Rev Neurol* **15**, 73–88 (2019).
6. Busche, M. A. et al. Decreased amyloid-beta and increased neuronal hyperactivity by immunotherapy in Alzheimer's models. *Nat Neurosci* **18**, 1725–1727 (2015).
7. Mably, A. J. et al. Anti-Abeta antibodies incapable of reducing cerebral Abeta oligomers fail to attenuate spatial reference memory deficits in J20 mice. *Neurobiol Dis* **82**, 372–384 (2015).
8. Walsh, D. M. & Selkoe, D. J. Amyloid beta-protein and beyond: the path forward in Alzheimer's disease. *Curr Opin Neurobiol* **61**, 116–124 (2020).
9. van Dyck, C. H. et al. Lecanemab in early Alzheimer's disease. *New Engl J Med* **388**, 9–21 (2022).
10. Busche, M. A. et al. Critical role of soluble amyloid-beta for early hippocampal hyperactivity in a mouse model of Alzheimer's disease. *Proc Natl Acad Sci USA* **109**, 8740–8745 (2012).
11. Liebscher, S., Keller, G. B., Goltstein, P. M., Bonhoeffer, T. & Hubener, M. Selective persistence of sensorimotor mismatch signals in visual cortex of behaving Alzheimer's Disease mice. *Curr Biol* **26**, 956–964 (2016).
12. Zarhin, D. et al. Disrupted neural correlates of anesthesia and sleep reveal early circuit dysfunctions in Alzheimer models. *Cell Rep* **38**, 110268 (2022).
13. Siskova, Z. et al. Dendritic structural degeneration is functionally linked to cellular hyperexcitability in a mouse model of Alzheimer's disease. *Neuron* **84**, 1023–1033 (2014).
14. Busche, M. A. et al. Clusters of hyperactive neurons near amyloid plaques in a mouse model of Alzheimer's disease. *Science* **321**, 1686–1689 (2008).
15. Bookheimer, S. Y. et al. Patterns of brain activation in people at risk for Alzheimer's disease. *N Engl J Med* **343**, 450–456 (2000).
16. Dickerson, B. C. et al. Increased hippocampal activation in mild cognitive impairment compared to normal aging and AD. *Neurology* **65**, 404–411 (2005).
17. Zott, B., Busche, M. A., Sperling, R. A. & Konnerth, A. What happens with the circuit in Alzheimer's disease in mice and humans? *Annu Rev Neurosci* **41**, 277–297 (2018).
18. Zott, B. et al. A vicious cycle of  $\beta$  amyloid-dependent neuronal hyperactivation. *Science* **365**, 559–565 (2019).
19. Palop, J. J. & Mucke, L. Network abnormalities and interneuron dysfunction in Alzheimer disease. *Nat Rev Neurosci* **17**, 777–792 (2016).
20. Keskin, A. D. et al. BACE inhibition-dependent repair of Alzheimer's pathophysiology. *Proc Natl Acad Sci USA* **114**, 8631–8636 (2017).
21. Richter, A., Eggenstein, E. & Skerra, A. Anticalins: exploiting a non-Ig scaffold with hypervariable loops for the engineering of binding proteins. *FEBS Lett* **588**, 213–218 (2014).

22. Rothe, C. & Skerra, A. Anticalin® proteins as therapeutic agents in human diseases. *BioDrugs* **32**, 233–243 (2018).
23. Rauth, S. et al. High-affinity Anticalins with aggregation-blocking activity directed against the Alzheimer beta-amyloid peptide. *Biochem J* **473**, 1563–1578 (2016).
24. Eichinger, A., Rauth, S., Hinz, D., Feuerbach, A. & Skerra, A. Structural basis of Alzheimer beta-amyloid peptide recognition by engineered lipocalin proteins with aggregation-blocking activity. *Biol Chem* **403**, 557–571 (2022).
25. Sturchler-Pierrat, C. et al. Two amyloid precursor protein transgenic mouse models with Alzheimer disease-like pathology. *Proc Natl Acad Sci USA* **94**, 13287–13292 (1997).
26. Kirkpatrick, D. C. & Wightman, R. M. Evaluation of drug concentrations delivered by microiontophoresis. *Anal Chem* **88**, 6492–6499 (2016).
27. Crespi, G. A. N., Hermans, S. J., Parker, M. W. & Miles, L. A. Molecular basis for mid-region amyloid- $\beta$  capture by leading Alzheimer's disease immunotherapies. *Sci Rep* **5**, 9649–9649 (2015).
28. Linse, S. et al. Kinetic fingerprints differentiate the mechanisms of action of anti-A $\beta$  antibodies. *Nat Struct Mol Biol* <https://doi.org/10.1038/s41594-020-0505-6> (2020).
29. Bouter, Y. et al. Abeta targets of the biosimilar antibodies of Bapineuzumab, Crenezumab, Solanezumab in comparison to an antibody against N-truncated Abeta in sporadic Alzheimer disease cases and mouse models. *Acta Neuropathologica* **130**, 713–729 (2015).
30. Abramowski, D. et al. Dynamics of Abeta turnover and deposition in different beta-amyloid precursor protein transgenic mouse models following gamma-secretase inhibition. *J Pharmacol Exp Ther* **327**, 411–424 (2008).
31. Li, S. et al. Soluble Abeta oligomers inhibit long-term potentiation through a mechanism involving excessive activation of extrasynaptic NR2B-containing NMDA receptors. *J Neurosci* **31**, 6627–6638 (2011).
32. Zott, B. & Konnerth, A. Impairments of glutamatergic synaptic transmission in Alzheimer's disease. *Sem Cell Dev Biol* <https://doi.org/10.1016/j.semcdb.2022.03.013> (2022).
33. Hefendehl, J. K. et al. Mapping synaptic glutamate transporter dysfunction in vivo to regions surrounding Abeta plaques by iGluSnFR two-photon imaging. *Nat Commun* **7**, 13441 (2016).
34. Aggarwal, A. et al. Glutamate indicators with improved activation kinetics and localization for imaging synaptic transmission. *bioRxiv*, 2022.2002.2013.480251 <https://doi.org/10.1101/2022.02.13.480251> (2022).
35. Unger, F., Konnerth, A. & Zott, B. Population imaging of synaptically released glutamate in mouse hippocampal slices. *STAR Protoc* **2**, 100877 (2021).
36. Shankar, G. M. et al. Amyloid-beta protein dimers isolated directly from Alzheimer's brains impair synaptic plasticity and memory. *Nat Med* **14**, 837–842 (2008).
37. O'Nuallain, B. et al. Amyloid beta-protein dimers rapidly form stable synaptotoxic protofibrils. *J Neurosci* **30**, 14411–14419 (2010).
38. Li, S. et al. Decoding the synaptic dysfunction of bioactive human AD brain soluble Abeta to inspire novel therapeutic avenues for Alzheimer's disease. *Acta Neuropathol Commun* **6**, 121 (2018).
39. Hong, W. et al. Diffusible, highly bioactive oligomers represent a critical minority of soluble Abeta in Alzheimer's disease brain. *Acta Neuropathol* **136**, 19–40 (2018).
40. LeVine, H. 3rd. Quantification of beta-sheet amyloid fibril structures with thioflavin T. *Methods Enzymol* **309**, 274–284 (1999).
41. Stine, W. B., Jungbauer, L., Yu, C. & LaDu, M. J. Preparing synthetic Abeta in different aggregation states. *Methods Mol Biol* **670**, 13–32 (2011).
42. Sengupta, U., Nilson, A. N. & Kaye, R. The Role of Amyloid- $\beta$  Oligomers in Toxicity, Propagation, and Immunotherapy. *EBioMedicine* **6**, 42–49 (2016).
43. Enache, T. A., Chiorcea-Paquim, A. M. & Oliveira-Brett, A. M. Amyloid-beta peptides time-dependent structural modifications: AFM and voltammetric characterization. *Anal Chim Acta* **926**, 36–47 (2016).
44. Sperling, R. A. et al. Functional alterations in memory networks in early Alzheimer's disease. *Neuromolecular Med* **12**, 27–43 (2010).
45. Grienberger, C. et al. Staged decline of neuronal function in vivo in an animal model of Alzheimer's disease. *Nat Commun* **3**, 774 (2012).
46. Kunz, L. et al. Reduced grid-cell-like representations in adults at genetic risk for Alzheimer's disease. *Science* **350**, 430–433 (2015).
47. Bakker, A. et al. Reduction of hippocampal hyperactivity improves cognition in amnesic mild cognitive impairment. *Neuron* **74**, 467–474 (2012).
48. O'Shea, S. D. et al. Intracerebroventricular administration of amyloid  $\beta$ -protein oligomers selectively increases dorsal hippocampal dialysate glutamate levels in the awake rat. *Sensors (Basel, Switzerland)* **8**, 7428–7437 (2008).
49. Brinkmalm, G. et al. Identification of neurotoxic cross-linked amyloid-beta dimers in the Alzheimer's brain. *Brain* **142**, 1441–1457 (2019).
50. Yang, T., Li, S., Xu, H., Walsh, D. M. & Selkoe, D. J. Large soluble oligomers of amyloid beta-protein from Alzheimer brain are far less neuroactive than the smaller oligomers to which they dissociate. *J Neurosci* **37**, 152–163 (2017).
51. Haass, C. & Steiner, H. Alzheimer disease gamma-secretase: a complex story of GxGD-type presenilin proteases. *Trends Cell Biol* **12**, 556–562 (2002).
52. Dovey, H. F. et al. Functional gamma-secretase inhibitors reduce beta-amyloid peptide levels in brain. *J Neurochem* **76**, 173–181 (2001).
53. Walsh, D. M., Tseng, B. P., Rydel, R. E., Podlisny, M. B. & Selkoe, D. J. The oligomerization of amyloid  $\beta$ -protein begins intracellularly in cells derived from human brain. *Biochemistry* **39**, 10831–10839 (2000).
54. Walsh, D. M. et al. Naturally secreted oligomers of amyloid beta protein potently inhibit hippocampal long-term potentiation in vivo. *Nature* **416**, 535–539 (2002).
55. Oddo, S. et al. Temporal profile of amyloid-beta (Abeta) oligomerization in an in vivo model of Alzheimer disease. A link between Abeta and tau pathology. *J Biol Chem* **281**, 1599–1604 (2006).
56. Koffie, R. M. et al. Oligomeric amyloid beta associates with postsynaptic densities and correlates with excitatory synapse loss near senile plaques. *Proc Natl Acad Sci USA* **106**, 4012–4017 (2009).
57. Sturchler-Pierrat, C. & Staufenbiel, M. Pathogenic mechanisms of Alzheimer's disease analyzed in the APP23 transgenic mouse model. *Ann N Y Acad Sci* **920**, 134–139 (2000).
58. Stosiek, C., Garaschuk, O., Holthoff, K. & Konnerth, A. In vivo two-photon calcium imaging of neuronal networks. *Proc Natl Acad Sci USA* **100**, 7319–7324 (2003).
59. Prinz, W. A., Aslund, F., Holmgren, A. & Beckwith, J. The role of the thioredoxin and glutaredoxin pathways in reducing protein disulfide bonds in the Escherichia coli cytoplasm. *J Biol Chem* **272**, 15661–15667 (1997).
60. Studier, F. W. & Moffatt, B. A. Use of bacteriophage T7 RNA polymerase to direct selective high-level expression of cloned genes. *J Mol Biol* **189**, 113–130 (1986).
61. Bachmann, B. J. Pedigrees of some mutant strains of Escherichia coli K-12. *Bacteriol Rev* **36**, 525–557 (1972).
62. Skerra, A., Pfützinger, I. & Plückthun, A. The functional expression of antibody Fv fragments in Escherichia coli: improved vectors and a generally applicable purification technique. *Bio/Technology* **9**, 273–278 (1991).
63. Fling, S. P. & Gregerson, D. S. Peptide and protein molecular weight determination by electrophoresis using a high-molarity tris buffer system without urea. *Anal Biochem* **155**, 83–88 (1986).

64. Gasteiger, E. et al. ExpASY: the proteomics server for in-depth protein knowledge and analysis. *Nucleic Acids Research* **31**, 3784–3788 (2003).
65. Marvin, J. S. et al. Stability, affinity, and chromatic variants of the glutamate sensor iGluSnFR. *Nat Methods* **15**, 936–939 (2018).
66. Ting, J. T. et al. Preparation of Acute Brain Slices Using an Optimized N-Methyl-D-glucamine Protective Recovery Method. *JoVE*, e53825 (2018).
67. Jia, H., Rochefort, N. L., Chen, X. & Konnerth, A. In vivo two-photon imaging of sensory-evoked dendritic calcium signals in cortical neurons. *Nature Protocols* **6**, 28–35 (2011).
68. Nimmerjahn, A. & Helmchen, F. In vivo labeling of cortical astrocytes with sulforhodamine 101 (SR101). *Cold Spring Harb Protoc* **2012**, 326–334 (2012).
69. Myszk, D. G. Improving biosensor analysis. *J Mol Recognit* **12**, 279–284 (1999).
70. Schonfeld, D. et al. An engineered lipocalin specific for CTLA-4 reveals a combining site with structural and conformational features similar to antibodies. *Proc Natl Acad Sci USA* **106**, 8198–8203 (2009).
71. Klunk, W. E. et al. Imaging A $\beta$  plaques in living transgenic mice with multiphoton microscopy and Methoxy-X04, a systemically administered congo red derivative. *J Neuropathol Exp Neurol* **61**, 797–805 (2002).
72. Benner, S., Kakeyama, M., Endo, T., Yoshioka, W. & Tohyama, C. Application of NeuroTrace staining in the fresh frozen brain samples to laser microdissection combined with quantitative RT-PCR analysis. *BMC Res Notes* **8**, 252 (2015).

## Acknowledgements

We thank C. Karrer, F. Beyer, S. Achatz and G. Finck for technical support. We are grateful to L. Looger for providing SF-iGluSnFR constructs. This work was funded by the German Research Foundation (DFG grant no. 685472) to BZ and the Max Planck School of Cognition. BZ is a is an Albrecht-Struppler-Clinician Scientist Fellow, funded by the Federal Ministry of Education and Research (BMBF) and the Free State of Bavaria under the Excellence Strategy of the Federal Government and the Länder, as well as by the Technical University of Munich - Institute for Advanced Study. AK is a Hertie-Senior-Professor for Neuroscience. MAB is supported by the UK Dementia Research Institute, which receives its funding from DRI Ltd., funded by the Medical Research Council, Alzheimer's Society and Alzheimer Research UK and by a UKRI Future Leaders Fellowship (grant number: MR/S017003/1).

## Author contributions

B.Z., A.S. and A.K. planned and oversaw all aspects of the study, B.Z., C.G., C.W., A.K-D and M.A.B performed and analyzed in vivo experiments, F.U. performed glutamate imaging experiments. M.M.K.

performed in vitro hippocampal calcium imaging. L.N. and A.F. purified and characterized the A $\beta$ -anticalin protein in vitro. B.Z., A.S. and A.K. wrote the manuscript with input and substantial revisions from all authors.

## Funding

Open Access funding enabled and organized by Projekt DEAL.

## Competing interests

A.S. is founder and shareholder of Pieris Pharmaceuticals, Inc. Anticalin<sup>®</sup> is a registered trademark of Pieris Pharmaceuticals GmbH, Germany. All other authors declare no competing interests.

## Additional information

**Supplementary information** The online version contains supplementary material available at <https://doi.org/10.1038/s41467-024-50153-y>.

**Correspondence** and requests for materials should be addressed to Benedikt Zott, Arne Skerra or Arthur Konnerth.

**Peer review information** *Nature Communications* thanks Colin Greineder, William Howe and the other, anonymous, reviewer for their contribution to the peer review of this work. A peer review file is available.

**Reprints and permissions information** is available at <http://www.nature.com/reprints>

**Publisher's note** Springer Nature remains neutral with regard to jurisdictional claims in published maps and institutional affiliations.

**Open Access** This article is licensed under a Creative Commons Attribution 4.0 International License, which permits use, sharing, adaptation, distribution and reproduction in any medium or format, as long as you give appropriate credit to the original author(s) and the source, provide a link to the Creative Commons licence, and indicate if changes were made. The images or other third party material in this article are included in the article's Creative Commons licence, unless indicated otherwise in a credit line to the material. If material is not included in the article's Creative Commons licence and your intended use is not permitted by statutory regulation or exceeds the permitted use, you will need to obtain permission directly from the copyright holder. To view a copy of this licence, visit <http://creativecommons.org/licenses/by/4.0/>.

© The Author(s) 2024